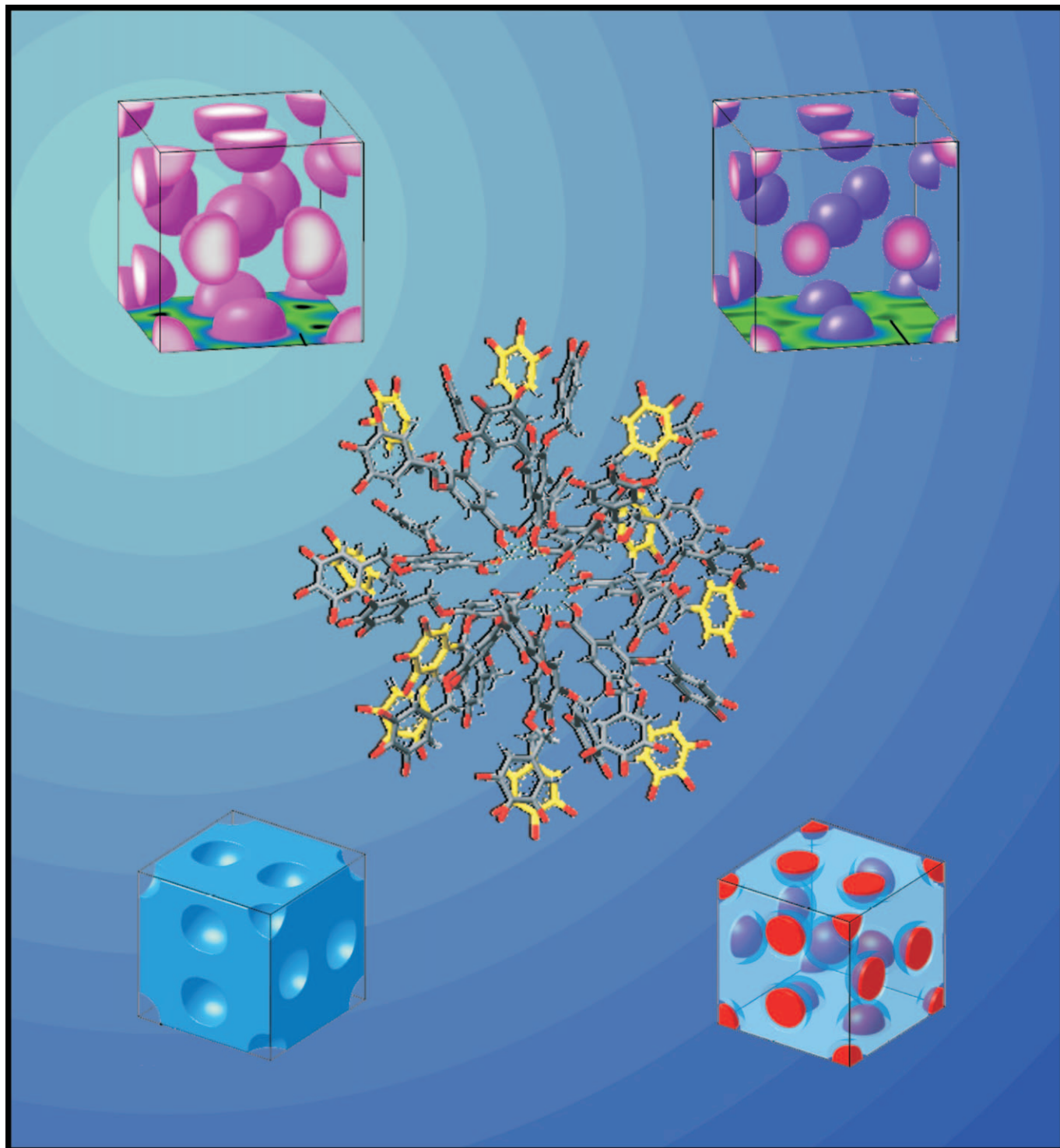


Elucidating the Structure of the $Pm\bar{3}n$ Cubic Phase of Supramolecular Dendrimers through the Modification of their Aliphatic to Aromatic Volume Ratio

Virgil Percec,*^[a] Mihai Peterca,^[a, b] Yusuke Tsuda,^[a] Brad M. Rosen,^[a] Satoshi Uchida,^[a] Mohammad R. Imam,^[a] Goran Ungar,^[c] and Paul A. Heiney^[b]



Abstract: The synthesis, and structural and retrostructural analysis of a library of second-generation conical dendrons that self-assemble into spherical supramolecular dendrimers is reported. This library consists of amphiphilic dendrons with *n*-alkyl groups containing from 4 to 16 carbon atoms. The dendrons containing 6 to 16 carbon atoms in their *n*-alkyl groups self-assemble into spherical supramolecular dendrimers that self-organize in a *Pm* $\bar{3}n$ cubic lattice. The structural and retrostructural analysis of the *Pm* $\bar{3}n$ lattices

generated from the supramolecular dendrimers demonstrated that the volume of the aromatic core of the spherical dendrimers is not dependent on the number of carbon atoms from their alkyl groups. This result facilitated the calculation of the average values of the absolute electron density of the aliphatic and aromatic domains

Keywords: cubic phase • dendrimers • liquid crystals • self-assembly • X-ray diffraction

of the spherical supramolecular dendrimers. The relative intensity of the higher order diffraction peaks of the *Pm* $\bar{3}n$ lattice increases as the volume of the aliphatic part of the sphere mediated by the number of carbon atoms in the *n*-alkyl groups decreases. This study demonstrates the maximum increase of the relative intensity of the higher order diffraction peaks of the *Pm* $\bar{3}n$ lattice generated from non-hollow supramolecular dendrimers.

Introduction

Amphiphilic benzyl ether dendrons prepared through conventional convergent iterative approaches^[1] with aliphatic groups on their periphery self-assemble and self-organize in a diversity of periodic^[2–4] and quasi-periodic^[2a,5] arrays. The primary structure of the dendron induces a preferred molecular conformation that controls the solid angle of the dendron.^[2g] As the solid angle increases, the self-assembly and self-organization process is gradually shifted from lamellar/smectic to columnar to spherical supramolecular structures.^[2k,q,r] Detailed structural and retrostructural analysis, including the application of helical diffraction theory,^[6] have guided the design of new functions based on dendrons predisposed to columnar self-assembly, such as: controlled reactivity,^[7] aquaporin mimics,^[8] self-repairing electronic materials,^[9] and nanomechanical actuators.^[10] The development of functional materials based upon spherical self-assembling dendrons is in an earlier stage. It has recently been observed that certain spherical self-assembling dendrons exhibit reduced electron density in their center,^[2s] thereby enabling the design of chiral and achiral spherical architectures containing a hollow center with potential for encapsulation and

delivery of molecular species.^[11] Amplification of chirality by supramolecular spheres is also an unprecedented event.^[11,12]

Further expansion of the role of spherical self-assembling dendrons as functional nanomaterials^[13] requires greater elaboration of their assembled structure and their relationship to lattice properties. While an impressive diversity of periodic cubic lattices have been documented for benzyl ether, phenylpropyl ether, and other aryl alkyl ether dendrons, including tetragonal *P4*/*mnm*,^[2n] body-centered cubic *Im* $\bar{3}m$,^[3] bicontinuous cubic *Ia* $\bar{3}d$,^[4] cubic *Pm* $\bar{3}n$,^[2s,14] and 12-fold liquid quasicrystal quasi-periodic arrays,^[2q,5] the *Pm* $\bar{3}n$ lattice is by far the most ubiquitous and was coincidentally first observed in soft-condensed matter in these systems.^[2d] Many aryl alkyl ether dendrons possess thermally reversible phase transitions between columnar and spherical assemblies. As temperature increases the molecular taper angle increases, resulting in a series of lattices. In such cases, the order of phases is typically hexagonal columnar *p6mm* → cubic *Pm* $\bar{3}n$ → tetragonal *P4*/*mnm* → body-centered cubic *Im* $\bar{3}m$.^[3a] Thus, the cubic *Pm* $\bar{3}n$ lattice exists at the border between columnar and spherical assemblies. Extensive work through transmission electron microscopy,^[2e] scanning force microscopy,^[7b] atomic force microscopy,^[2h] and isomorphous replacement^[2l] was required to definitively establish a spherical model as opposed to an interlocked columnar model for the *Pm* $\bar{3}n$ lattice.

While many aspects of the relationship between the structure of self-assembling aryl alkyl ether dendrons and the *Pm* $\bar{3}n$ lattices they form have been elaborated, critical questions remain. Of particular interest is the nature of the aromatic core structure and the minimum number of carbon atoms in the alkyl groups that are needed to form a supramolecular sphere. For example, in the pioneering publication on the cubic *Pm* $\bar{3}n$ lattice it was considered that a minimum of 12 carbon atoms in the alkyl group is needed to generate the spherical assemblies.^[2d] Further, one signature used to distinguish hollow from filled spheres in the *Pm* $\bar{3}n$ cubic phase is the relative enhancement of the higher order

[a] Prof. V. Percec, Dr. M. Peterca, Prof. Y. Tsuda, B. M. Rosen, Prof. S. Uchida, Dr. M. R. Imam
Roy & Diana Vagelos Laboratories
Department of Chemistry, University of Pennsylvania
Philadelphia, Pennsylvania, 19104-6323 (USA)
Fax: (+1) 215-573-7888
E-mail: percec@sas.upenn.edu

[b] Dr. M. Peterca, Prof. P. A. Heiney
Department of Physics and Astronomy
University of Pennsylvania, Philadelphia
Pennsylvania, 19104-6396 (USA)

[c] Prof. G. Ungar
Department of Engineering Materials
University of Sheffield, Mappin Street
Sheffield S1 3JD (UK)

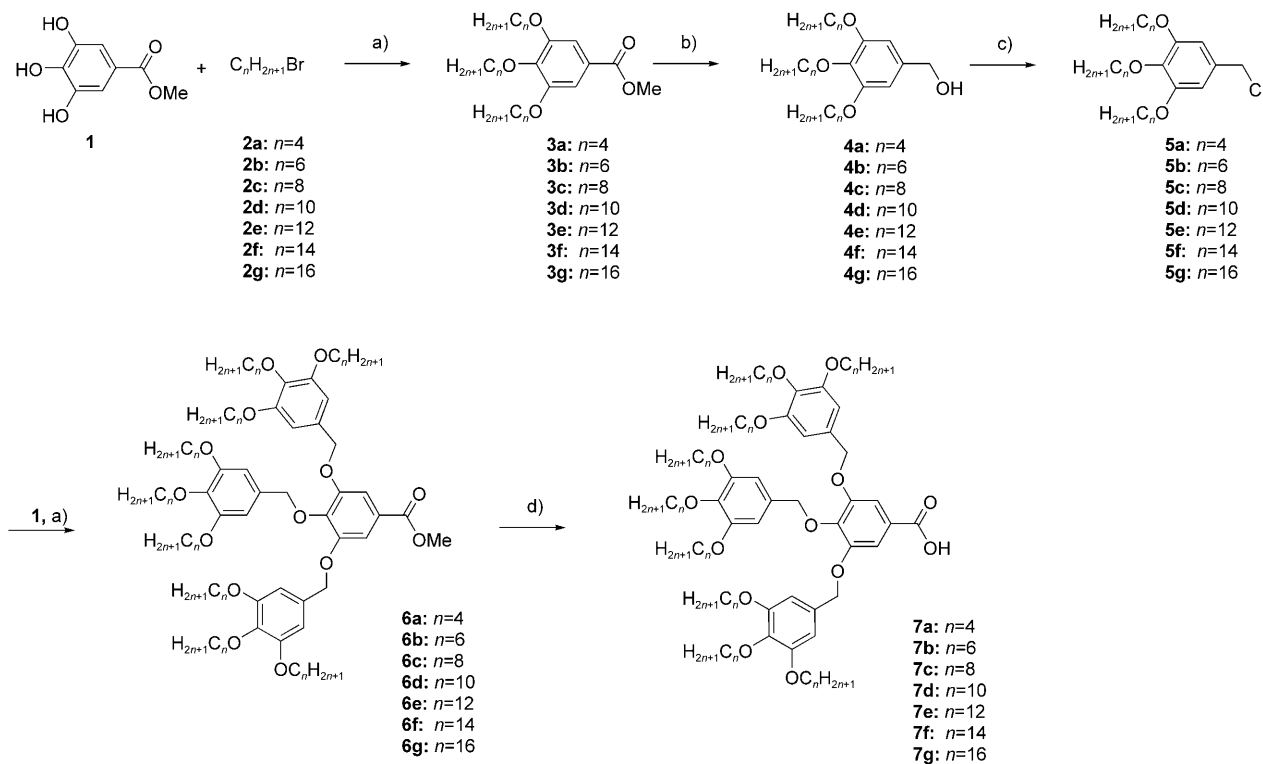
 Supporting information for this article is available on the WWW under <http://dx.doi.org/10.1002/chem.200901324>.

X-ray powder diffraction peaks. One cause of such enhancement is the variation of the electron-density at the hollow center boundary. However, the ratio between the aliphatic and aromatic domains could also affect the higher order peak intensities.^[11] As hollow spheres and filled spheres would be targeted for dramatically different functions, it is essential to be able to definitively distinguish between these two structures. Both of these questions relating to the fundamental structure of the aromatic core are addressed in this study through the synthesis and structural analysis of seven dendritic acids, in which the number of methylenic units in the aliphatic periphery was varied, (Scheme 1). Structural and retrostructural analysis demonstrated that the aromatic core contains a constant number of dendrons regardless of tail length, suggesting that the packing of the aromatic region is preserved. From this, we were able to calculate a specific molecular and supramolecular conformation of the aromatic core. These results can be used to evaluate the structure of other spherical self-assembling dendrons. As the dendritic acids chosen in this study self-assemble into filled supramolecular spherical structures that self-organize into the *Pm*3*n* cubic phase, it is possible to single out the role played by the aliphatic region in the amplification of higher order X-ray diffraction peaks. In this work we perform a systematic variation of the aliphatic groups from six to sixteen carbon atoms to establish the effect of a change in aromatic to aliphatic volume ratio on the formation of this cubic phase and on the relative intensity of the higher order

X-ray powder diffraction peaks. This investigation demonstrates that spherical supramolecular dendrimers self-assemble with an unexpectedly large range of the number of carbon atoms in the alkyl groups (six to sixteen), in contrast to the previous estimate.^[2d] In addition, powder diffraction simulations were used to demonstrate that the enhancement of higher order XRD amplitudes, (Table 1), is caused by the faster spatial variation of the electron density in the supramolecular dendrimers with a thinner aliphatic shell. The observed increase of the relative intensity of the higher order X-ray powder diffraction peaks is at least three times smaller than the increase observed for hollow supramolecular spheres self-assembled from other benzyl ether dendrons.^[2s,11] This result definitively demonstrates that for the previously reported hollow supramolecular spheres only a fraction of the observed enhancement was generated by the reduction of the number of carbon atoms from the alkyl groups. Finally, a model for the aromatic core of the supramolecular sphere was calculated for the first time.

Results and Discussion

Synthesis: The seven dendritic acids investigated in this study were synthesized according to iterative procedures described previously (Scheme 1).^[2e] Methyl 3,4,5-trihydroxybenzoate (**1**) was etherified with either *n*-bromobutane (**2a**), *n*-bromohexane (**2b**), *n*-bromoocctane (**2c**), *n*-bromodecane



Scheme 1. Synthesis of the second-generation (3,4,5)²G2-COOH (**7a-7g**) series of dendritic acids. Reagents and conditions: a) K_2CO_3 , DMF, 65°C ; b) LiAlH_4 , Et_2O ; c) SOCl_2 , CH_2Cl_2 ; d) KOH , EtOH , reflux.

Table 1. Structural and retro-structural analysis for the $(3,4,5)^2n$ G2-COOH (**7a–7g**) library of dendritic acids self-assembled into $Pm\bar{3}n$ cubic phase.

$n^{[a]}$	$A_{200}^{[b]}$ [a.u.]	$A_{210}^{[b]}$ [a.u.]	$A_{211}^{[b]}$ [a.u.]	$A_{220}^{[b]}$ [a.u.]	$A_{320}^{[b]}$ [a.u.]	$A_{321}^{[b]}$ [a.u.]	$A_{400}^{[b]}$ [a.u.]	$M_{wt}^{[c]}$	$a_{90^\circ C}^{[d]}$ [Å]	$a_{110^\circ C}^{[d]}$ [Å]	$\rho^{[e]}$ [g cm $^{-3}$]	$\mu_{90^\circ C}^{[f]}$	$\mu_{110^\circ C}^{[f]}$	$V_{aliph}^{[g]}$ [%]	$V_{arom}^{[h]}$ [%]
6	111.4	100.0	89.1	11.4	21.2	26.3	45.0	1341.9	58.1	57.7	1.03	11.3	11.1	57.12	42.88
8	109.0	100.0	87.7	8.3	17.7	21.4	32.5	1594.4	62.2	61.4	1.02	11.6	11.1	63.91	36.09
10	106.9	100.0	85.6	9.9	7.9	14.8	23.8	1846.8	66.1	65.2	1.00	11.8	11.3	68.85	31.15
12	110.1	100.0	84.2	9.2	— ^[i]	7.8	21.7	2099.3	70.5	68.5	1.00	12.5	11.5	72.59	27.41
14	106.7	100.0	83.4	— ^[i]				2351.8	72.7	71.6	0.99	12.2	11.6	75.53	24.47
16	107.2	100.0	83.4	— ^[i]				2604.3	75.5	74.6	0.99	12.3	11.9	77.91	22.09

[a] Number of C atoms in the alkyl periphery. [b] A_{hk} : (hkl) relative scaled diffraction peak amplitude, calculated after applying the multiplicity and Lorentz corrections. [c] Dendron molecular weight. [d] Experimental lattice parameter of the $Pm\bar{3}n$ cubic phase calculated at the indicated temperatures. [e] Experimental density measured at 20°C. [f] Number of dendrons per supramolecular cluster at two representative temperatures calculated using $\mu = \rho a^3 N_A / (8 M_{wt})$, in which $N_A = 6.022 \times 10^{23}$ (mol $^{-1}$) = Avogadro number. [g] Aliphatic volume fraction calculated from the molecular structure using $V_{aliph} = 9 M_{tail}/M_{wt}$, in which M_{tail} = molecular weight of one ($C_{2n}H_{2n+1}$) n -alkyl chain. [h] Aromatic volume fraction calculated from the molecular structure using $V_{arom} = 1 - V_{aliph}$. [i] X-ray diffraction peak with weak intensity, (i.e. intensity comparable with the background level).

(**2d**), *n*-bromododecane (**2e**), *n*-bromotetradecane (**2f**), or *n*-bromohexadecane (**2g**) in DMF at 65°C. The resulting methyl trisalkoxybenzoates ($(3,4,5)^2n$ G1-COO*Me* (**3a–3g**) were reduced with LiAlH₄ to form the corresponding benzyl alcohols ($(3,4,5)^2n$ G1-CH₂OH (**4a–4g**). Chlorination with SOCl₂ furnished benzyl chlorides ($(3,4,5)^2n$ G1-CH₂Cl (**5a–5g**). Second-generation benzyl ether dendrons ($(3,4,5)^2n$ G2-COO*Me* (**6a–6g**) were prepared by alkylation of the precursor benzyl chloride with methyl 3,4,5-trihydroxybenzoate in DMF at 65°C. Basic hydrolysis with KOH in EtOH provided the dendritic acids ($(3,4,5)^2n$ G2-COOH (**7a–7g**).

Structural and retrostructural analysis: The structural and retrostructural analysis of the library of dendritic acids involves solution NMR spectroscopy, differential scanning calorimetry, small- and wide-angle powder X-ray diffraction, molecular modeling, and reconstruction and simulation^[11] of the three-dimensional electron density distribution.

The differential scanning calorimetric experiments revealed that the dendritic acid with $n=4$ is the only one from the series that does not exhibit a thermotropic $Pm\bar{3}n$ cubic phase. From $n=6$ to 16 the $Pm\bar{3}n$ cubic mesophase is observed in all supramolecular structures assembled at high temperature. We note that, upon the increase of n from 6 to 8 and to 10, the isotropization transition temperature shifts to slightly higher values. As n is further increased, from 10 to 12, 14, and to 16 (Figure 1), the isotropization transition temperature shifts to slightly lower values. Overall, these shifts are small, demonstrating that the increase of n has a relative small impact on the thermodynamics of the self-assembly process. Therefore, the interactions within the aromatic region are dominant, even though their volume fraction is reduced from $V_{arom}=42.88\%$ for $n=6$ to $V_{arom}=22.09\%$ for $n=16$ (Table 1).

The temperature dependence of the $Pm\bar{3}n$ cubic phase lattice parameter, a , is summarized in Figure 2. For all the dendritic acids investigated the temperature variation of a is small. For example, in the case of $n=8$ the lattice parameter a decreased with less than 3% in between 20 and 110°C. As a consequence, the calculated number of dendrons, μ listed in Table 1, that self-assemble to form the supramolecular dendrimers in the $Pm\bar{3}n$ cubic phase, exhibits a small varia-

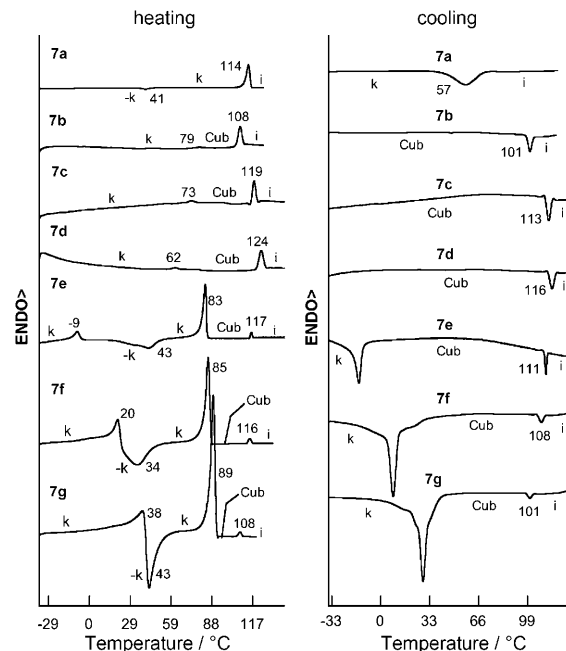


Figure 1. Second heating and cooling differential scanning calorimetric (DSC) traces of **7a–7g** series of dendritic acids. Transition temperatures in °C and phases are indicated; k: unidentified crystal phases, Cub: $Pm\bar{3}n$ cubic phase; i: isotropic phase.

tion with temperature. This suggests that the number of dendrons in the spherical aggregates does not change with the temperature. In fact for supramolecular spherical dendrimers such a change would be highly energetically unfavorable, as it would require a disruption of the dendrimer core aromatic to aromatic interactions. As the temperature is increased, the diameter of the supramolecular dendrimers decreases slightly (Table 1), most probably due to the “melting” of paraffinic chains that contributes to a better packing of the aliphatic region. This thermal process changes the density of the system and therefore can account for the small variations of μ listed in Table 1.

Table 1 also shows that the calculated value of μ is also quite insensitive to the length of the alkyl chain. For example, upon the increase of n from 6 to 16, μ varies from 11.1 to 11.9 (Table 1), a negligible increase that is well within the

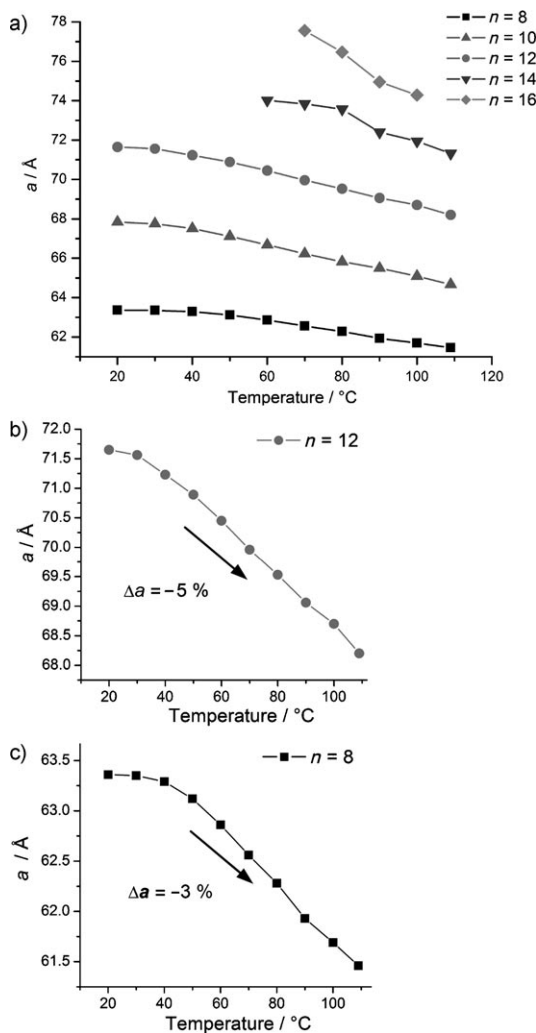


Figure 2. Temperature dependence of the lattice parameter a of the $Pm\bar{3}n$ phase generated from **7a–7g** (a) and detailed plots for **7c** $n=8$ (b) and **7e** $n=12$ (c).

experimental error. Furthermore, the linear dependence of the third power of the lattice dimension as a function of the number of methylenic units in the paraffinic chains (Figure 3) demonstrates that the number of dendrons that self-assemble into the supramolecular dendrimers of the $Pm\bar{3}n$ cubic phase must be the same for this library. This linear dependence allows us to extrapolate the value of the $Pm\bar{3}n$ lattice parameter to the case of a dendritic acid with no alkyl periphery. This value is approximately 37.9 Å (Figure 3) and it will be used later in the calculation of the average absolute electron density.

Influence of the aliphatic to aromatic volume ratio: Recent studies on amphiphilic dendritic architectures have suggested a correlation between the relative intensity of the higher order diffraction peaks and the size of the aliphatic region for both columnar and cubic phases.^[11] In these cases, the influence of the alkyl region thickness on the X-ray powder diffraction intensity profile could not be separated from the

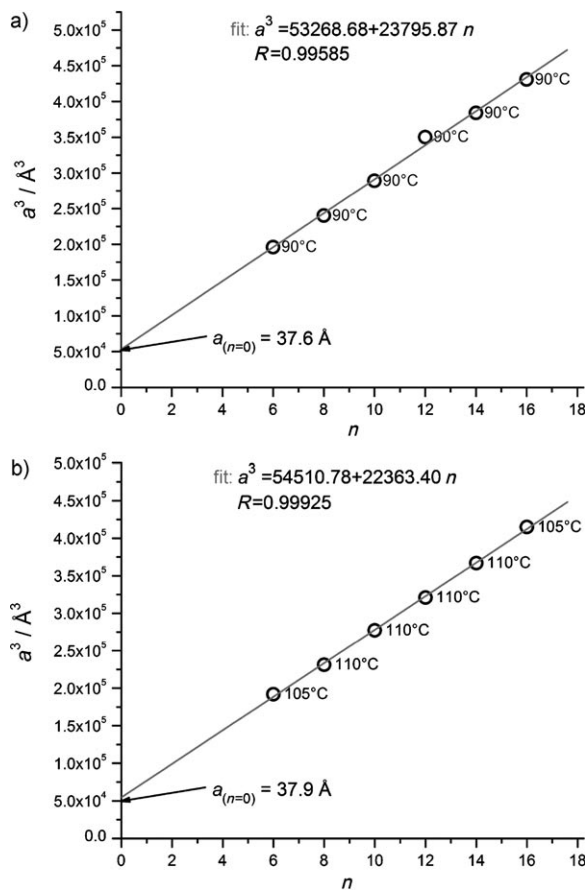


Figure 3. Third power of the $Pm\bar{3}n$ phase lattice dimension a^3 of **7a–7g** as a function of n at two representative temperatures. The fitted parameters and estimated lattice dimension of the $a_{n=0}$ dendron are shown.

role of the aromatic region due to the presence of a larger or smaller region of low electron density at the center of the supramolecular columns or spheres. In the present case, such low electron density regions are not present, simplifying the task of elucidating the influence of the aliphatic to aromatic region volume fraction on the X-ray powder diffraction intensity profile.

In Figure 4 the relative intensities of the $Pm\bar{3}n$ cubic phase powder diffraction peaks are indicated for the $n=8$ and $n=12$ dendritic acids. The data are scaled to the amplitude of the (210) diffraction peak. Table 1 lists the scaled diffraction peak amplitudes for the complete library. The amplitudes listed are calculated from the X-ray powder diffraction peaks area, after applying the appropriate Lorentz and multiplicity corrections. In general, upon decreasing the length of the alkyl chains, the relative intensity of the higher order X-ray diffraction peaks increases.

The reconstructed relative electron density distributions, calculated by Fourier series reconstruction from the amplitudes listed in Table 1, are presented in volumetric representation in Figure 4a for $n=8$ and in Figure 4b for $n=12$. The electron density reconstruction highlights the aromatic–aliphatic phase segregation,^[2d,5,11] as indicated by the electron density histograms calculated for the $Pm\bar{3}n$ unit cell and

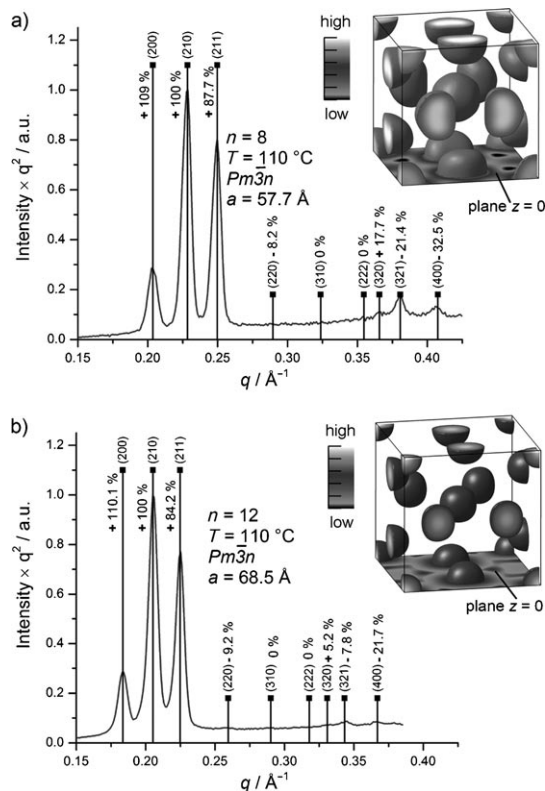


Figure 4. Powder diffraction intensity versus q plots collected at 110°C for **7c** $n=8$ (a) and **7e** $n=12$ (b). Diffraction peak positions, scaled amplitudes (with assigned phases + or -) and corresponding three-dimensional relative electron density reconstruction shown for one unit cell in volumetric representation are indicated. For clarity, only the highest electron density regions are shown.

shown in Figure 5d, e, and f. There is a distinct difference in the shapes of the high electron density regions for the two dendritic acids compared in Figure 4: the $n=8$ self-assembled dendrimers are more distorted from spherical symmetry than those self-assembled from $n=12, 14$, or 16 dendritic acids. These differences, together with the unit cell distribution of the relative electron density, are illustrated in Figure 5. Note that the electron density scales, although normalized separately between the minimum and maximum density for each individual compound, are nevertheless approximately comparable as the minima and maxima correspond roughly to the aliphatic and aromatic electron density, respectively. These values are similar for all the dendritic acids (Table 2). As expected, the fractional volume occupied by the high electron density regions decreases as the length of the alkyl chain is increased, (Figure 5d, e, f). This is also apparent from the blunt density maxima in **7c**, that is, the large white areas in Figure 5a and the sharp cutoff at the high-density end of the histogram in Figure 5d. The volume fraction values from Figure 5d, e and f reflect these architectural changes, and they are calculated based on the chemical structure, as shown in Table 2.

We now discuss the origin of the enhancement of the higher order X-ray diffraction peak amplitudes observed

upon the decrease of n . There are three possibilities: 1) the enhancement may be due to a higher degree of positional order that follows from the reduction of the conformational freedom in the structures with lower n ; 2) the reduction of the aliphatic region thickness may change the actual value of the aliphatic region electron density, enhancing the aliphatic to aromatic electron density contrast; or 3) the shorter alkyl chains may cause a faster spatial change of the electron density triggering the enhancement. The first possibility is difficult to address. In a later section, it will be demonstrated that the powder XRD data can be simulated without the need of introducing the extra parameters required to take into account such sphere-sphere disorder. Therefore this possibility cannot be completely excluded, but the XRD simulations demonstrate that the role played by long-range correlations is not dominant.

To evaluate the second option, we extrapolate the lattice parameter to a putative $n=0$ dendritic acid (Table 2) to calculate the absolute average electron density of the aromatic and of the aliphatic regions for this library of dendritic acids. Table 1 demonstrates that, within the experimental error, the number of dendrons that self-assemble into the supramolecular dendrimers of the $Pm\bar{3}n$ cubic phase is independent of the temperature or the alkyl chain length. This indicates that the electron density in the aromatic region of the $n=6$ to 16 dendritic acids is the same (Figure 3 and 5, Table 2). This result is then used to calculate the absolute electron density of the aliphatic region for all the dendritic acids listed in Table 2. The calculated average values of the absolute electron densities of $0.5 \text{ e}\text{\AA}^{-3}$ for the aromatic region and of $0.3 \pm 0.02 \text{ e}\text{\AA}^{-3}$ for the aliphatic region are in the range observed for similar structures already reported.^[14] Similar average electron densities were calculated independent of the shape or size of the supramolecular clusters, for example, $\rho_{\text{arom}} = 0.49 \text{ e}\text{\AA}^{-3}$ and $\rho_{\text{aliph}} = 0.28 \text{ e}\text{\AA}^{-3}$ for the $n=6$ compound, (caption Table 2). Thus, the changes in aliphatic region electron density are negligible, and we can exclude the second option.

We are thus lead to the third explanation for the enhancement of the higher order diffraction peak amplitudes. The calculated dimensions and electron densities for the aromatic and aliphatic regions of the self-assembled supramolecular dendrimers are presented in Figure 6a. We use the published^[11] ideal spherical or distorted spherical model to calculate the X-ray powder diffraction patterns. We considered a two-level model illustrated in Figure 6b, consisting of spherical or distorted spherical shells of constant electron densities for the aromatic regions embedded in an aliphatic continuum. Using the calculated values of average absolute electron densities and diameters of the aliphatic and aromatic region, the powder diffraction simulations in Figure 6c, d, and e show that, indeed, the faster spatial variation of the electron density is the primary factor in the enhancement of the higher order diffraction peaks amplitudes. In other words, the decrease of n generates faster spatial changes that trigger more non-zero Fourier components and a gradual increase of their weight in the XRD patterns. In a

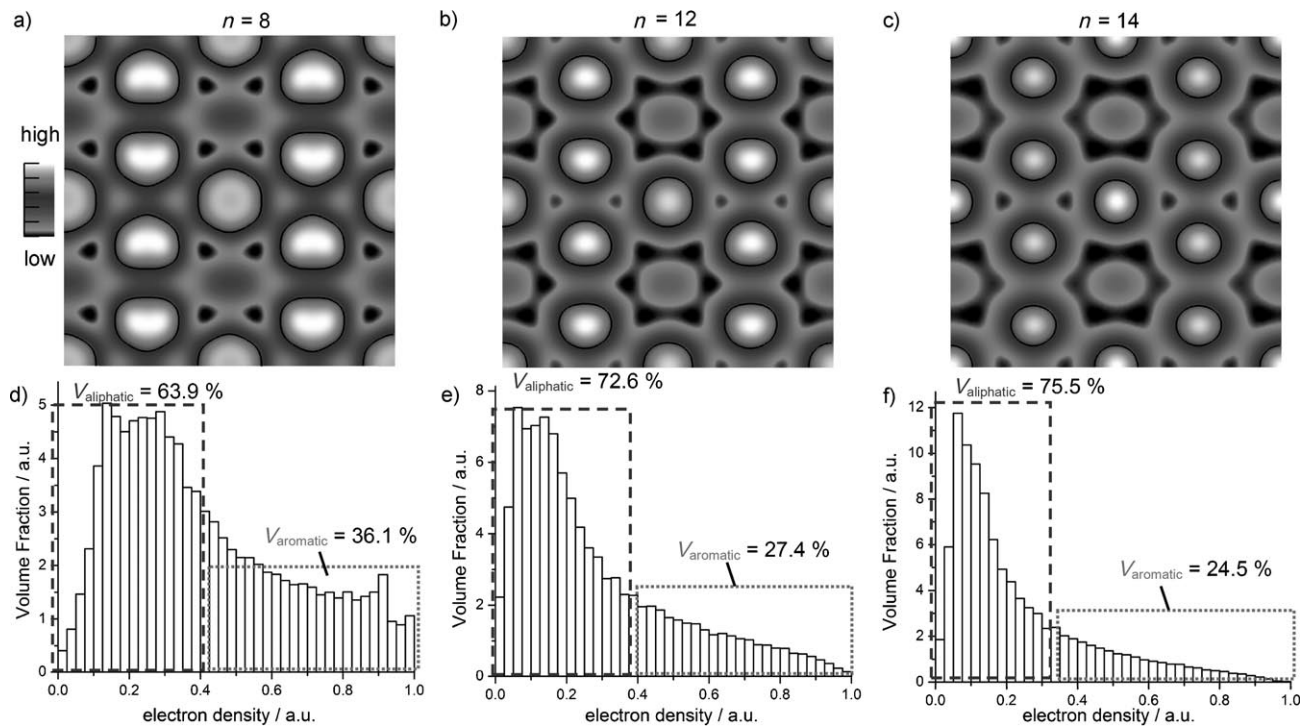


Figure 5. Reconstructed relative electron density two-dimensional maps of the plane $z=0$ (a, b, c) and the corresponding histograms calculated from the three-dimensional volumetric electron density distribution of the $Pm\bar{3}n$ unit cell (d, e, f) of **7a–7g**. In a), b), and c) for clarity the maps are shown for a 2×2 unit cell; in d), e), and f) the rectangles approximate the volume fraction occupied by the aliphatic (dashed rectangles) and aromatic (dotted rectangles) regions as calculated in Table 2.

simplified way the distribution presented in Figure 6a can be envisioned as being similar to a series of slits forming a

Table 2. Average electron densities in the aromatic and aliphatic region of the $(3,4,5)^2nG2-COOH$ (**7a–7g**) library of dendritic acids self-assembled into $Pm\bar{3}n$ cubic phase.

$n^{[a]}$	$N_{\text{arom}}^{[b]}$	$R_{\text{arom}}^{[c]}$	$\rho_{\text{arom}}^{[d]}$	$N_{\text{aliph}}^{[e]}$	$R_{\text{aliph}}^{[f]}$	$\rho_{\text{aliph}}^{[g]}$
6	295	11.65	0.51	441	18.01	0.28
8	295	11.65	0.51	585	19.26	0.29
10	295	11.65	0.51	729	20.21	0.30
12	295	11.65	0.51	873	21.22	0.30
14	295	11.65	0.51	1017	22.19	0.29
16	295	11.65	0.51	1161	23.12	0.29

[a] Number of methylenic units in the alkyl chain. [b] N_{arom} =number of electrons in the aromatic region of the dendron calculated using $N_{\text{arom}}=6_c \times 28 + 8_o \times 14 + 1_H \times 15 = 295$ e⁻. [c] R_{arom} =calculated aromatic region radii using $R_{\text{arom}} = 37.9 \times \sqrt[3]{3/(32\pi)} = 11.65$ Å, in which 37.9 Å is the estimated lattice dimension for the $n=0$ dendron (Figure 3). [d] ρ_{arom} =calculated average electron density of the supramolecular cluster aromatic region using $\rho = \mu N_{\text{arom}}(4\pi R_{\text{arom}}^3/3)$, in which μ is the average number of dendrons per supramolecular cluster (Table 1). [e] N_{aliph} =number of electrons in the aliphatic region of the dendron calculated using $N_{\text{aliph}} = 9[6_c n + 1_H(2n+1)]$. [f] R_{aliph} =calculated aliphatic region radii using $R_{\text{aliph}} = a \times \sqrt[3]{3/(32\pi)}$, in which a is the experimental lattice parameter (Table 1). [g] ρ_{aliph} =calculated average electron density of the supramolecular cluster aliphatic region using $\rho = \mu N_{\text{aliph}}(4\pi R_{\text{aliph}}^3/3)$. Remark: similar average electron densities values were calculated from the unit cell volume without any spherical shaped approximation; for example for $n=6$ the calculated values are $\rho_{\text{arom}} = \mu_{\text{cell}} N_{\text{arom}} a^{-3} = 8 \times 11.09 \times 295 \times 37.9^{-3} = 0.49$ e⁻ Å⁻³ and $\rho_{\text{aliph}} = \mu_{\text{cell}} N_{\text{aliph}} (a^3 - a_{\text{arom}}^3)^{-1} = 8 \times 11.1 \times 441 \times (57.7^3 - 37.9^3)^{-1} = 0.28$ e⁻ Å⁻³.

diffraction grating in optical experiments. In this case it is easy to understand the correlation between the slit separation or width and the optical diffraction intensity profile.

The fitted aromatic radii, 11.6–12.7 Å as indicated in Figure 6b for $n=6$, 8, and 12, are close to the calculated value of $R_{\text{arom}} = 11.65$ Å, Table 2. The fitted distortion from the spherical symmetry of the dendrimers on the faces of the unit cell varies from 0.89 for $n=12$ to 0.86 for $n=6$ and 8, (a value of 1.00 corresponds to a sphere and a value smaller than 1.00 corresponds to an oblate spheroid^[11]). These values are in agreement with the reconstructed electron density maps shown in Figure 5 that highlight an increased deviation from spherical symmetry to an oblate spheroid shape of the dendrimers on the faces of the unit cell as n is reduced.

Structure of the supramolecular dendrimers: In the previous sections it was demonstrated that the number of dendrons that self-assemble into the supramolecular dendrimers of the presented $Pm\bar{3}n$ cubic phase is independent both of temperature changes and of the size of the aliphatic region. The reconstructed electron density distributions in Figures 4 and 5 demonstrate that powder X-ray diffraction can yield detailed information about the size and shape of the aromatic region. Moving the level of the isoelectron surface from low to high density in the three-dimensional maps in Figure 4 can be thought of as peeling away layer after layer of atoms from the aliphatic region. The results presented imply that the aromatic core of the dendrimers on the faces of the unit

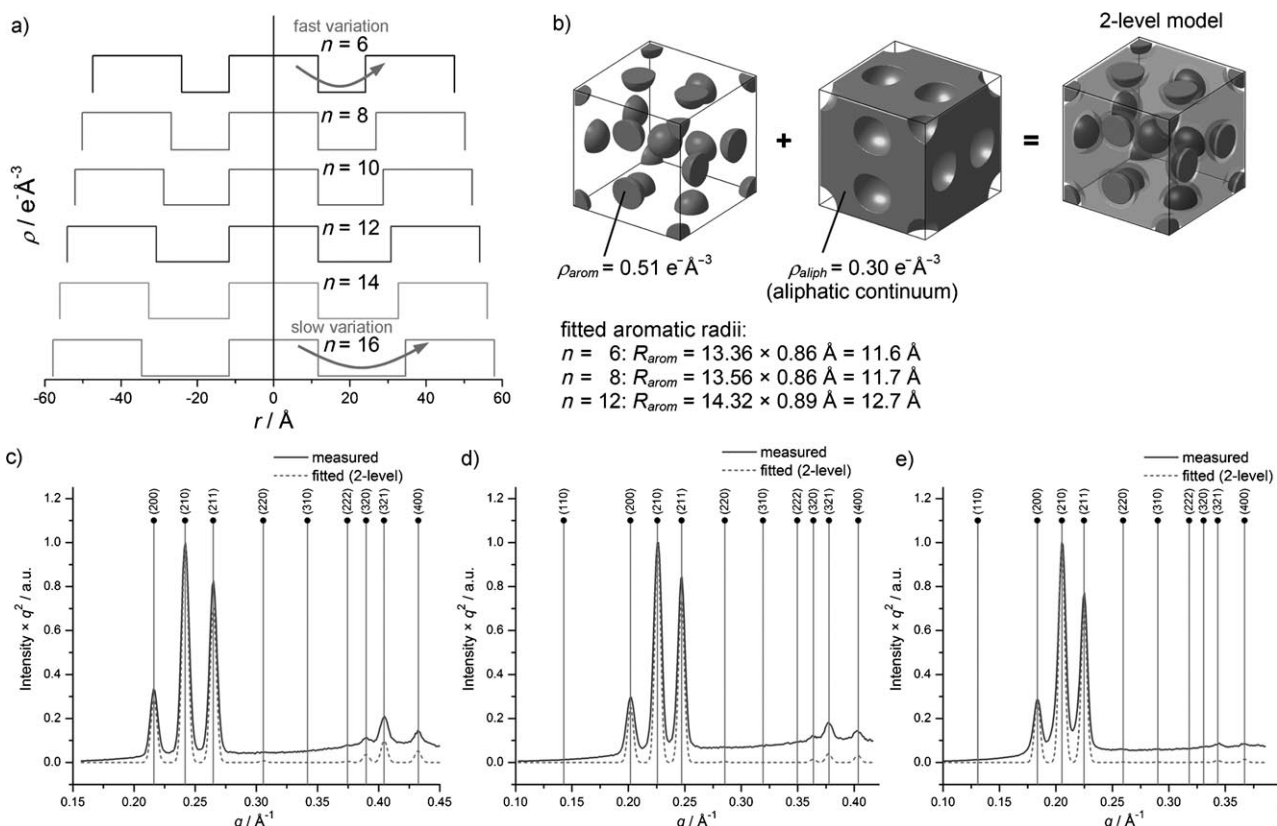


Figure 6. a) Average electron density (ρ) for the aromatic and aliphatic region (Table 2) plotted along the face clusters close contact direction, for clarity the plots are y axis shifted. b) The two-level model of constant electron densities used to simulate the powder XRD intensities. c), d), and e) Measured and two-level fitted X-ray diffraction plots for **7b**, **7c**, and **7e**, respectively; no background was subtracted from the measured plots.

cell, as indicated in Figure 7b, is slightly larger and more distorted than the aromatic core of the supramolecular dendrimers at the corners and the center. Furthermore, the Voronoi polyhedral space filling representation of the $Pm\bar{3}n$ unit cell shown in Figure 7b illustrates the slightly larger volume occupied by the “face” dendrimers in comparison with the “corner/center” ones.^[11]

It is clear that the number of dendrons in a spherical supramolecular dendrimer must be an integer. The average number of dendrons in the $Pm\bar{3}n$ unit cell of the investigated dendritic acid library is approximately 92 (Table 1, Figure 7). We combine these observations to conclude that the “face” supramolecular dendrimer is self-assembled from twelve dendrons and the “corner/center” one from ten, as shown in Figure 7b. Density functional theory, together with ^1H NMR experiments,^[2d] demonstrated the most probable conformation of the dendron in the supramolecular dendrimers of the $Pm\bar{3}n$ cubic phase. In Figure 7a the proposed molecular model illustrates that the 4-aromatic substitution is in an orthogonal conformation with respect with the core phenyl. The two outer 3- and 5-aromatic substituted phenyls adopt a symmetric tilted conformation with respect with the core aromatic phenyl. The aromatic core region of the supramolecular dendrimer self-assembled from twelve dendrons is shown in Figure 7c in stick-view and in Figure 7d in

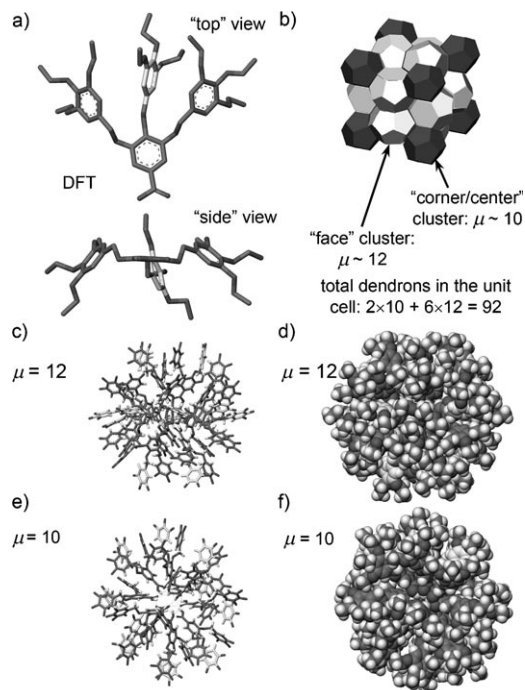


Figure 7. Molecular model of the supramolecular sphere self-assembled from **7a–7g**: a) DFT conformation; b) number of dendrons per supramolecular dendrimer and per unit cell; c) and e) detail of the aromatic core region; d) and f) supramolecular dendrimer in space-filling view.

space filling view, while that of the supramolecular dendrimers self-assembled from ten dendrons in Figure 7e and f.

Conclusions

The systematic investigation of a library of dendritic acids as a function of the number of methylenic units in the paraffinic groups revealed the structure of the spherical supramolecular dendrimers that self-organize into the $Pm\bar{3}n$ cubic phase. This is the cubic phase most often encountered during the self-assembly of amphiphilic dendrons or dendrimers. The combination of electron density reconstruction, experimental density and molecular modeling demonstrated that there are two types of supramolecular dendrimers in this phase, as already reported for other libraries.^[2s,11] For the presented library it was shown that for the $Pm\bar{3}n$ cubic phases the corner spherical supramolecular dendrimers self-assembled from ten dendrons and the face distorted spherical dendrimers are self-assembled from twelve dendrons. The preferred structure of the dendron of the supramolecular dendrimer was predicted by DFT methods and provides insight into the molecular arrangement of the aromatic-core of spherical dendrimers. Moreover, the present study revealed the extent to which the change in spatial variation in electron density, generated by the variation of the aromatic to aliphatic volume fraction, can increase the relative intensity of the higher order X-ray diffraction peaks of the $Pm\bar{3}n$ cubic phase. In relative scaled amplitudes the (400) peak intensity was shown here to increase to at most 45% of the (210) peak. For hollow supramolecular dendrimers the value was reported to range from 100% to 170%, for dendrons with similar aliphatic to aromatic volume ratios.^[11] A comparison of these numbers demonstrates that, without a hollow center, the relative amplitudes of the high order diffraction peaks are at least three times less intense, suggesting that a definitive assignment to hollow phases can be made in cases of such large amplifications. Finally, for the first time, this study provides the average absolute electron densities of the aliphatic and aromatic regions of amphiphilic dendrons, namely, $0.5 \text{ e } \text{\AA}^{-3}$ and $0.3 \pm 0.02 \text{ e } \text{\AA}^{-3}$ respectively. These values are critical for the accurate modeling of dendrimer lattices, a key step in the retrostructural analysis of self-assembling dendrons.

Experimental Section

Materials: Al_2O_3 (activated, basic, Brockmann I, standard grade, ~150 mesh, 58 Å) and silica gel (ICN EcoChrom Silitech 23–63 D 60 Å) was used as received. Et_2O (Fisher, A.C.S. reagent grade) was refluxed over sodium benzophenone ketyl and distilled freshly before use. LiAlH_4 (95+%), SOCl_2 (99+%), methyl 3,4,5-trihydroxybenzoate (98%), *n*-bromobutane, *n*-bromohexane, *n*-bromoocetane, *n*-bromodecane, *n*-bromododecane, *n*-bromotetradecane, and *n*-bromohexadecane (all from Aldrich) were used as received. Anhydrous K_2CO_3 , KOH, EtOH, DMF, and CH_2Cl_2 (all A.C.S. reagent grade, from Fisher) were used as received.

General methods: ^1H NMR (360 MHz) and ^{13}C NMR (90 MHz) spectra were recorded on a Bruker AC-360 instrument. Thin-layer chromatography (TLC) was performed by using precoated TLC plates (silica gel with F_{254} indicator; layer thickness, 200 µm; particle size 5–25 µm; pore size 60 Å, SIGMA-Aldrich). MALDI-TOF-MS was performed on the Voyager-DE PRO Biospectrometry Workstation with 2,5-dihydroxybenzoic acid as a matrix. A Perkin-Elmer Series 10 HPLC equipped with an LC-100 column oven, Nelson Analytical 900 Series integrator data station, and two Perkin-Elmer PL gel columns of 5×10^2 and $1 \times 10^4 \text{ \AA}$ was used in both HPLC and GPC mode. THF was used as solvent at the oven temperature of 40°C unless otherwise noted. Detection was by UV absorbance at 254 nm. Polystyrene standards ($1.02 \leq M_w/M_n \leq 1.13$) were used to construct the calibration curve. Thermal transitions were measured on a Perkin-Elmer DSC-7. Zn and In were used as calibration standards. In all cases, the heating and cooling rates were $10^\circ\text{C min}^{-1}$ unless otherwise noted. First-order transition temperatures were reported as the maxima and minima of their endothermic and exothermic peaks. Glass transition temperatures (T_g) were read at the middle of the change in heat capacity. X-ray diffraction (XRD) measurements were performed using $\text{Cu}_{\text{K}\alpha}$ radiation ($\lambda = 1.54178 \text{ \AA}$) from a Bruker-Nonius FR-591 rotating anode X-ray source equipped with a $0.2 \times 0.2 \text{ mm}^2$ filament operated at 3.4 kW. The Cu radiation beam was collimated and focused by a single bent mirror and sagitally focused through a Si (111) monochromator, generating in a $0.3 \times 0.4 \text{ mm}^2$ spot on a Bruker-AXS Hi-Star multiwire area detector. To minimize attenuation and background scattering, an integral vacuum was maintained along the length of the flight tube and within the sample chamber. Samples were held in thin-wall glass capillaries (0.7–1.0 mm in diameter), mounted in a temperature-controlled oven (temperature precision: $\pm 0.1^\circ\text{C}$, temperature range from –120 to 270°C). The distance between the sample and the detector was 12.0 cm for wide angles diffraction experiments and 54.0 cm for intermediate angles diffraction experiments respectively. XRD peaks position and intensity analysis was performed using Datasqueeze Software (version 2.01) that allows background elimination and Gaussian, Lorentzian, Lorentzian squared, or Voigt peak-shape fitting.

Computational techniques: All calculations were performed using the Spartan'06 Quantum Mechanics Program (PC/X86).^[16] To obtain the predicted self-assembled conformation of **7a–7g**, a molecular mechanics conformation distribution for a test compound bearing shortened alkyl tails, $(3,4,5)^2\text{G}_2\text{-COOH}$, was generated at the MMFF level. Of the 1728 benzyl linkage conformers examined the 100 hundred unique conformations generated were inspected for relative energy and symmetry. Full geometry optimizations of the lowest energy structures and those bearing appropriate symmetry for spherical self-assembly were performed at the B3LYP/6-31G* level. The optimized geometries were subjected to single-point energy and frequency calculations at the B3LYP/6-31G* level, to confirm that there were no imaginary modes and that the structures were true local minima and not merely saddle points.

Synthesis: The detailed synthesis and characterization of the second-generation **7a–7g** series of dendritic acids can be found in the Supporting Information.

Acknowledgements

Financial support by the National Science Foundation (DMR-0548559 and DMR-0520020) and the P. Roy Vagelos Chair at University of Pennsylvania is gratefully acknowledged. B.M.R. gratefully acknowledge the financial support from American Chemical Society—Division of Organic Chemistry Graduate Research Fellowship, sponsored by Roche, Inc.

[1] a) *Dendrimers and Other Dendritic Polymers* (Eds.: J. M. J. Fréchet, D. A. Tomalia), Wiley, New York, 2001; b) G. R. Newkome, C. N. Moorefield, F. Vögtle, *Dendrimers and Dendrons*, Wiley-VCH, Weinheim, 2001.

- [2] a) V. Percec, G. Johansson, J. Heck, G. Ungar, S. V. Batty, *J. Chem. Soc. Perkin Trans. I* **1993**, 1411–1420; b) G. Johansson, V. Percec, G. Ungar, D. Abramic, *J. Chem. Soc. Perkin Trans. I* **1994**, 447–459; c) V. Percec, G. Johansson, G. Ungar, J. Zhou, *J. Am. Chem. Soc.* **1996**, 118, 9855–9866; d) V. S. K. Balagurusamy, G. Ungar, V. Percec, G. Johansson, *J. Am. Chem. Soc.* **1997**, 119, 1539–1555; e) S. D. Hudson, H.-T. Jung, V. Percec, W. D. Cho, G. Johansson, G. Ungar, V. S. K. Balagurusamy, *Science* **1997**, 278, 449–452; f) V. Percec, W.-D. Cho, P. E. Mosier, G. Ungar, D. J. P. Yeadley, *J. Am. Chem. Soc.* **1998**, 120, 11061–11070; g) G. Ungar, V. Percec, M. N. Holerca, G. Johansson, J. A. Heck, *Chem. Eur. J.* **2000**, 6, 1258–1266; h) V. Percec, W.-D. Cho, M. Möller, S. A. Prokhorova, G. Ungar, D. J. P. Yeadley, *J. Am. Chem. Soc.* **2000**, 122, 4249–4250; i) V. Percec, W.-D. Cho, G. Ungar, *J. Am. Chem. Soc.* **2000**, 122, 10273–10281; j) V. Percec, W. D. Cho, G. Ungar, D. J. P. Yeadley, *Angew. Chem.* **2000**, 112, 1661–1666; *Angew. Chem. Int. Ed.* **2000**, 39, 1597–1602; k) V. Percec, W. D. Cho, G. Ungar, D. J. P. Yeadley, *J. Am. Chem. Soc.* **2001**, 123, 1302–1315; l) D. R. Dukeson, G. Ungar, V. S. K. Balagurusamy, V. Percec, G. A. Johansson, M. Glodde, *J. Am. Chem. Soc.* **2003**, 125, 15974–15980; m) V. Percec, M. Glodde, G. Johansson, V. S. K. Balagurusamy, P. A. Heiney, *Angew. Chem.* **2003**, 115, 4474–4478; *Angew. Chem. Int. Ed.* **2003**, 42, 4338–4342; n) G. Ungar, Y. S. Liu, X. B. Zeng, V. Percec, W. D. Cho, *Science* **2003**, 299, 1208–1211; o) V. Percec, C. M. Mitchell, W. D. Cho, S. Uchida, M. Glodde, G. Ungar, X. Zeng, Y. Liu, V. S. K. Balagurusamy, P. A. Heiney, *J. Am. Chem. Soc.* **2004**, 126, 6078–6094; p) V. Percec, M. N. Holerca, S. Nummelin, J. J. Morrison, M. Glodde, J. Smidrkal, M. Peterca, B. M. Rosen, S. Uchida, V. S. K. Balagurusamy, M. J. Sienkowska, P. A. Heiney, *Chem. Eur. J.* **2006**, 12, 6216–6241; q) V. Percec, M. Peterca, M. J. Sienkowska, M. A. Ilies, E. Aqad, J. Smidrkal, P. A. Heiney, *J. Am. Chem. Soc.* **2006**, 128, 3324–3334; r) V. Percec, J. Smidrkal, M. Peterca, C. M. Mitchell, S. Nummelin, A. E. Dulcey, M. J. Sienkowska, P. A. Heiney, *Chem. Eur. J.* **2007**, 13, 3989–4007; s) V. Percec, B. C. Won, M. Peterca, P. A. Heiney, *J. Am. Chem. Soc.* **2007**, 129, 11265–11278.
- [3] a) D. J. P. Yeadley, G. Ungar, V. Percec, M. N. Holerca, G. Johansson, *J. Am. Chem. Soc.* **2000**, 122, 1684–1689; b) C. J. Jang, J. H. Ryu, J. D. Lee, D. Sohn, M. Lee, *Chem. Mater.* **2004**, 16, 4226–4231; c) S. Coco, C. Cordovilla, B. Donnio, P. Espinet, M. J. Garcia-Casas, D. Guillou, *Chem. Eur. J.* **2008**, 14, 3544–3552.
- [4] a) P. Massiot, M. Imperor-Clerc, M. Veber, R. Deschenaux, *Chem. Mater.* **2005**, 17, 1946–1951; b) S. N. Chvalun, M. A. Shcherbina, A. N. Yakunin, J. Blackwell, V. Percec, *Vysokomol. Soedin. Ser. A* **2007**, 49, 266–278; *Polym. Sci. Ser. A* **2007**, 49, 158–167.
- [5] X. Zeng, G. Ungar, Y. Liu, V. Percec, A. E. Dulcey, J. K. Hobbs, *Nature* **2004**, 428, 157–160.
- [6] a) W. Cochran, F. H. C. Crick, V. Vand, *Acta Crystallogr.* **1952**, 5, 581–586; b) M. Peterca, V. Percec, M. R. Imam, P. Leowanawat, K. Morimitsu, P. A. Heiney, *J. Am. Chem. Soc.* **2008**, 130, 14840–14852.
- [7] a) V. Percec, C. H. Ahn, B. Barboiu, *J. Am. Chem. Soc.* **1997**, 119, 12978–12979; b) V. Percec, J. G. Rudick, M. Peterca, M. Wagner, M. Obata, C. M. Mitchell, W. D. Cho, V. S. K. Balagurusamy, P. A. Heiney, *J. Am. Chem. Soc.* **2005**, 127, 15257–15264; c) V. Percec, C. H. Ahn, G. Ungar, D. J. P. Yeadley, M. Moller, S. S. Sheiko, *Nature* **1998**, 391, 161–164; d) V. Percec, M. N. Holerca, *Biomacromolecules* **2000**, 1, 6–16.
- [8] a) V. Percec, A. E. Dulcey, V. S. K. Balagurusamy, Y. Miura, J. Smidrkal, M. Peterca, S. Nummelin, U. Edlund, S. D. Hudson, P. A. Heiney, D. A. Hu, S. N. Magonov, S. A. Vinogradov, *Nature* **2004**, 430, 764–768; b) V. Percec, A. E. Dulcey, M. Peterca, M. Ilies, J. Ladiraslaw, B. M. Rosen, U. Edlund, P. A. Heiney, *Angew. Chem.* **2005**, 117, 6674–6679; *Angew. Chem. Int. Ed.* **2005**, 44, 6516–6521; c) V. Percec, A. Dulcey, M. Peterca, M. Ilies, Y. Miura, U. Edlund, P. A. Heiney, *Aust. J. Chem.* **2005**, 58, 472–482; d) V. Percec, A. E. Dulcey, M. Peterca, M. Ilies, M. J. Sienkowska, P. A. Heiney, *J. Am. Chem. Soc.* **2005**, 127, 17902–17909; e) V. Percec, A. E. Dulcey, M. Peterca, M. Ilies, S. Nummelin, M. J. Sienkowska, P. A. Heiney, *Proc. Natl. Acad. Sci. USA* **2006**, 103, 2518–2523; f) M. Peterca, V. Percec, A. E. Dulcey, S. Nummelin, S. Korey, M. Ilies, P. A. Heiney, *J. Am. Chem. Soc.* **2006**, 128, 6713–6720; g) V. Percec, A. E. Dulcey, M. Peterca, P. Adelman, R. Samant, V. S. K. Balagurusamy, P. A. Heiney, *J. Am. Chem. Soc.* **2007**, 129, 5992–6002; h) M. S. Kaucher, M. Peterca, A. E. Dulcey, A. J. Kim, S. A. Vinogradov, D. A. Hammer, P. A. Heiney, V. Percec, *J. Am. Chem. Soc.* **2007**, 129, 11698–11699.
- [9] a) V. Percec, M. Glodde, T. K. Bera, Y. Miura, I. Shiyanskaya, K. D. Singer, V. S. K. Balagurusamy, P. A. Heiney, I. Schnell, A. Rapp, H.-W. Spiess, S. D. Hudson, H. Duan, *Nature* **2002**, 417, 384–387; b) V. Percec, M. Glodde, M. Peterca, A. Rapp, I. Schnell, H.-W. Spiess, T. K. Bera, Y. Miura, V. S. K. Balagurusamy, E. Aqad, P. A. Heiney, *Chem. Eur. J.* **2006**, 12, 6298–6314; c) V. Percec, E. Aqad, M. Peterca, M. R. Imam, M. Glodde, T. K. Bera, Y. Miura, V. S. K. Balagurusamy, P. C. Ewbank, F. Wurthner, P. A. Heiney, *Chem. Eur. J.* **2007**, 13, 3330–3345; d) V. Duzhko, K. D. Singer, E. Aqad, M. Peterca, M. R. Imam, V. Percec, *Appl. Phys. Lett.* **2008**, 92, 113312.
- [10] a) J. G. Rudick, V. Percec, *New J. Chem.* **2007**, 31, 1083–1096; b) V. Percec, J. G. Rudick, M. Peterca, P. A. Heiney, *J. Am. Chem. Soc.* **2008**, 130, 7503–7508; c) J. G. Rudick, V. Percec, *Macromol. Chem. Phys.* **2008**, 209, 1759–1768; d) J. G. Rudick, V. Percec, *Acc. Chem. Res.* **2008**, 41, 1641–1652.
- [11] V. Percec, M. Peterca, A. E. Dulcey, M. R. Imam, S. D. Hudson, S. Nummelin, P. Adelman, P. A. Heiney, *J. Am. Chem. Soc.* **2008**, 130, 13079–13094.
- [12] a) V. Percec, M. R. Imam, M. Peterca, D. A. Wilson, P. A. Heiney, *J. Am. Chem. Soc.* **2009**, 131, 1294–1304; b) V. Percec, M. R. Imam, M. Peterca, D. A. Wilson, R. Graf, H. W. Spiess, V. S. K. Balagurusamy, P. A. Heiney, *J. Am. Chem. Soc.* **2009**, 131, 7662–7677.
- [13] a) J. S. Moore, *Acc. Chem. Res.* **1997**, 30, 402–413; b) Y. Kim, S. C. Zimmerman, *Curr. Opin. Chem. Biol.* **1998**, 2, 733–742; c) D. Seebach, P. B. Rheiner, G. Greiveldinger, T. Butz, H. Sellner, *Top. Curr. Chem.* **1998**, 197, 125–164; d) J.-P. Majoral, A.-M. Caminade, *Top. Curr. Chem.* **1998**, 197, 79–124; e) D. K. Smith, F. Diederich, *Chem. Eur. J.* **1998**, 4, 1353–1361; f) M. Fischer, F. Vögtle, *Angew. Chem.* **1999**, 111, 934–955; *Angew. Chem. Int. Ed.* **1999**, 38, 885–905; g) A. W. Bosman, H. M. Janssen, E. W. Meijer, *Chem. Rev.* **1999**, 99, 1665–1688; h) D. Astruc, F. Chardac, *Chem. Rev.* **2001**, 101, 2991–3024; i) R. Haag, *Chem. Eur. J.* **2001**, 7, 327–335; j) S. Hecht, J. M. J. Fréchet, *Angew. Chem.* **2001**, 113, 76–94; *Angew. Chem. Int. Ed.* **2001**, 40, 74–91; k) D. C. Tully, J. M. J. Fréchet, *Chem. Commun.* **2001**, 1229–1239; l) S.-E. Stiriba, H. Frey, R. Haag, *Angew. Chem.* **2002**, 114, 1385–1390; *Angew. Chem. Int. Ed.* **2002**, 41, 1329–1334; m) R. Esfand, D. A. Tomalia, *Drug Discovery Today* **2001**, 6, 427–436; n) E. R. Gillies, J. M. J. Fréchet, *Drug Discovery Today* **2005**, 10, 35–43; o) D.-L. Jiang, T. Aida, *Prog. Polym. Sci.* **2005**, 30, 403–422; p) R. Van de Coevering, R. J. M. K. Gebbink, G. Van Koten, *Prog. Polym. Sci.* **2005**, 30, 474–490; q) A.-M. Caminade, J.-P. Majoral, *Prog. Polym. Sci.* **2005**, 30, 491–505; r) U. Boas, P. M. H. Heegaard, *Chem. Soc. Rev.* **2004**, 33, 43–63; s) M. W. Grinstaff, *Chem. Eur. J.* **2002**, 8, 2838–2846; t) S. M. Grayson, J. M. J. Fréchet, *Chem. Rev.* **2001**, 101, 3819–3867; u) M. Marcos, R. Martín-Rapún, A. Omenat, J. Barberá, J. L. Serrano, *Chem. Mater.* **2006**, 18, 1206–1212; v) R. I. Gearba, D. V. Anokhin, A. I. Bondar, W. Bras, M. Jahr, M. Lehmann, D. A. Ivanov, *Adv. Mater.* **2007**, 19, 815–820; w) R. Mezzenga, J. Ruokolainen, N. Canilho, E. Kasémi, D. A. Schlüter, W. B. Lee, G. H. Fredrickson, *Soft Matter* **2009**, 5, 92–97.
- [14] a) B. K. Cho, A. Jain, S. M. Gruner, U. Wiesner, *Science* **2004**, 305, 1598–1601; b) T. Kato, T. Matsuoka, M. Nishii, Y. Kamiakawa, K. Kanie, T. Nishimura, E. Yamashita, S. Ujiie, *Angew. Chem.* **2004**, 116, 2003–2006; *Angew. Chem. Int. Ed.* **2004**, 43, 1969–1972; c) I. Bury, B. Heinrich, C. Bourgogne, D. Guillon, B. Donnio, *Chem. Eur. J.* **2006**, 12, 8396–8413; d) S. H. Seo, J. H. Park, G. N. Tew, J. Y. Chang, *Tetrahedron Lett.* **2007**, 48, 6839–6844; e) P. Fuchs, C. Tschiesske, K. Raith, K. Das, S. Diele, *Angew. Chem.* **2002**, 114, 650–653 *Angew. Chem. Int. Ed.* **2002**, 41, 628–631.
- [15] D. C. Turner, S. M. Gruner, *Biochemistry* **1992**, 31, 1340–1355.

- [16] Y. Shao, L. F. Molnar, Y. Jung, J. Kussmann, C. Ochsenfeld, S. T. Brown, A. T. B. Gilbert, L. V. Slipchenko, S. V. Levchenko, D. P. O'Neill, R. A. DiStasio, R. C. Lochan, T. Wang, G. J. O. Beran, N. A. Besley, J. M. Herbert, C. Y. Lin, T. Van Voorhis, S. H. Chien, A. Sodt, R. P. Steele, V. A. Rassolov, P. E. Maslen, P. P. Korambath, R. D. Adamson, B. Austin, J. Baker, E. F. C. Byrd, H. Dachsel, R. J. Doerkens, A. Dreuw, B. D. Dunietz, A. D. Dutoi, T. R. Furlani, S. R. Gwaltney, A. Heyden, S. Hirata, C. P. Hsu, G. Kedziora, R. Z. Khaliulin, P. Klunzinger, A. M. Lee, M. S. Lee, W. Liang, I. Lotan, N. Nair, B. Peters, E. I. Proynov, P. A. Pieniazek, Y. M. Rhee, J. Ritchie, E. Rosta, C. D. Sherrill, A. C. Simmonett, J. E. Subotnik, H. L. Woodcock, W. Zhang, A. T. Bell, A. K. Chakraborty, D. M. Chipman, F. J. Keil, A. Warshel, W. J. Hehre, H. F. Schaefer, J. Kong, A. I. Krylov, P. M. W. Gill, M. Head-Gordon, *Phys. Chem. Chem. Phys.* **2006**, *8*, 3172–3191.
- [17] V. Percec, C. H. Ahn, W. D. Cho, A. M. Jamieson, J. Kim, T. Leman, M. Schmidt, M. Gerle, M. Moller, S. A. Prokhorova, S. S. Sheiko, S. Z. D. Cheng, A. Zhang, G. Ungar, D. J. P. Yeardley, *J. Am. Chem. Soc.* **1998**, *120*, 8619–8631.

Received: May 18, 2009

Published online: August 26, 2009